PAPER

Orbit modeling of fast particle redistribution induced by sawtooth instability

To cite this article: D. Kim *et al* 2018 *Nucl. Fusion* **58** 082029

View the article online for updates and enhancements.

ORBIT modeling of fast particle redistribution induced by sawtooth instability

D. Kim[1] , M. Podestà[1] , D. Liu[2] and F.M. Poli[1]

[1] Princeton Plasma Physics Laboratory, Princeton, NJ 08543, United States of America
[2] Department of Physics and Astronomy, University of California, Irvine, CA 92617, United States of America

E-mail: dkim@pppl.gov

CrossMark

Abstract

Initial tests on the National Spherical Torus Experiment Upgrade (NSTX-U) (Menard *et al* 2012 *Nucl. Fusion* 083015) device suggest that introducing energy selectivity for sawtooth induced fast ion redistribution is required to improve the agreement between experimental and simulated quantities such as neutron rate and Fast-Ion D-Alpha profiles. The aim of this work is to assess the requirements to properly describe the behaviour of fast ions during a sawtooth crash for predictive sawtooth simulations. As the first step, in this work, we use the particle-following ORBIT code to characterize the redistribution of fast particles. In order for a sawtooth crash to be simulated, a spatial and temporal displacement is implemented into the ORBIT code. The perturbation amplitude is determined by comparison with experimental measurement of the neutron rate drop. The characteristics of fast ions with different orbit types are investigated in phase and real space. Due to a sawtooth crash, fast ion energy and angular momentum are modified resulting in the redistribution in phase space and orbit type change. The redistribution of fast ions in real space shows that the sawtooth instability brings different effect on fast particles with different orbit types as observed in experiments. The initial interpretative TRANSP simulation using the so-called *kick model* based on the ORBIT modeling result shows an improvement of fast ion redistribution before and after a sawtooth crash but the neutron rate still has discrepancy compared to the experimental measurement.

Keywords: NSTX-U, sawtooth, fast particle redistribution, ORBIT

(Some figures may appear in colour only in the online journal)

1. Introduction

The sawtooth instability in tokamak plasmas is characterized by periodic fast relaxations of plasma parameters, e.g. electron temperature and density, followed by a slower recovery in the central region where the safety factor q is below unity [1]. The sawtooth instability generally brings moderate confinement degradations but a sawtooth crash with a long period can lower the β limit for triggering neoclassical tearing modes (NTMs) [2], possibly leading to disruptions. Sawtooth crashes can also affect the transport of thermal plasma particles and fast ions (e.g. α-particles and particles from auxiliary heating systems). The population of particles is redistributed during the crash due to the reconnection of magnetic flux surface. Unlike for thermal particles, the effect of sawtooth crash on

fast ions depends on the characteristic of particle such as energy and orbit type, which needs to be taken into account for sawtooth modeling to understand and to interpret quantitatively the experimental results.

The National Spherical Torus Experiment-Upgrade (NSTX-U) [3] is equipped with two neutral beam (NB) injectors capable of injecting up to 12 MW of total NB power at maximum energy 95 keV. The first NB line injects with a deposition profile that is typically peaked on-axis [4], while the second NB line is injecting tangentially for off-axis NB current drive. Along with the upgrade of the central solenoid, which results in a four-fold increase of the available ohmic flux, the increased available NB power enables longer pulses on NSTX-U than previously achievable on NSTX [5]. Sawtoothing L-mode discharges lasting about 2 s were readily

obtained during the 2016 campaign [6], thus providing well-reproducible discharges to investigate sawtooth physics in a spherical torus.

The tokamak transport code TRANSP [7] enables time-dependent integrated simulations of a tokamak discharge. The code can be used to interpret existing experiments, as well as to develop new scenarios or make predictions for future devices (e.g. ITER). The NSTX-U sawtoothing discharges can be analyzed using the sawtooth model in TRANSP. The reconnection of magnetic flux surfaces is described using full reconnection (Kadomtsev) [8] or partial/incomplete reconnection (Porcelli) model [1] with free parameters such as reconnection fraction for partial reconnection case. For the thermal particles, in an interpretative simulation case, the input profiles already include the effect of sawtooth crash as they are reconstructed at the calculation time step while the redistribution of fast ions from NB needs to be described by the sawtooth model. For both cases, the sawtooth model is applied for q and poloidal magnetic flux redistribution. From interpretative TRANSP simulations including only the thermal ion density redistribution, neutron rate drops at each sawtooth crash time show 50% or larger difference from the experimental measurement, while other simulations applying the sawtooth model for fast ions can reproduce the experimental neutron rate drops [9].

In order for the TRANSP simulation to match the experimental data, a proper set of free parameters needs to be used. Thus it is difficult to apply the sawtooth model for a predictive simulation since the optimum parameter setting cannot be self-consistently determined. In addition, even though the neutron rate drops can be matched with a free parameter set, estimated features of fast ions can be different from the experimental ones. For instance, the distribution of fast ions obtained from FIDA (Fast Ion D-Alpha) [10, 11] measurement in figures 1(*a*) and (*b*) shows the drop and the increase in the post-crash profile inside and outside the inversion radius. However, in FIDA simulations [12] that use input profiles from TRANSP simulations that match the neutron rate drops, the post-crash profile is lower than the pre-crash profile across the minor radius [9].

A Monte Carlo approach is used in TRANSP to describe the dynamic of energetic particles. After a sawtooth crash, a fraction of the markers (pre-selected by the user) is displaced based on the pre-crash helical flux label characterizing each marker. Magnetic moment and parallel velocity are assumed to be conserved, whereas perpendicular velocity (hence, pitch) and energy are updated based on the local magnetic field at the displaced location. Since markers are assumed to be displaced only based on the match between their pre- versus post-crash helical fluxes, any velocity space dependence of fast particle redistribution is neglected in the TRANSP simulation. However, the latter is shown to be important from both experiments [9] and theoretical work [13].

Therefore, in order for the TRANSP simulation to be more quantitative to interpret sawtoothing discharges, an improved model to manage the redistribution of fast ions during a sawtooth crash needs to be developed. The model needs to take into account the energy, toroidal angular momentum and

pitch of fast ions, which affect the redistribution of fast ions in phase and real spaces. Implementation of such model into TRANSP would enable interpretative sawtooth simulations to validate the model by comparison with experimental measurements from NSTX-U or other conventional tokamaks, not only in terms of neutron rate drop but also for profiles such as fast ion density profile. After that it will be possible to have a more comprehensive predictive model for the fast particle redistribution induced by sawtooth crashes beyond simple zero-dimensional theoretical predictions.

In this paper, as the first step, simulations using the Hamiltonian guiding center code ORBIT [14] are carried out. ORBIT simulations can be used as a guidance to develop a more comprehensive model for characterizing the fast particle redistribution by sawteeth as the dependence of characteristics of fast ion are taken into account in the simulation. The experimental scenario of the target discharge is summarized in section 2. A perturbation model implemented into the ORBIT code to represent the sawtooth instability is introduced in section 3 with the comparison with the experimentally measured neutron rate drop for the determination of the mode amplitude. In section 4, the characteristic of fast ion redistribution is investigated for different orbit types and particle energy and initial result of the application of *kick model* [15, 16] based on the ORBIT simulations to TRANSP simulation is shown. Finally, the conclusion follows in section 5.

2. Experimental scenario

The discharge analyzed in this work (NSTX-U #204083 L-mode sawtoothing discharge with 1 MW injected NB power) is shown in figure 2. Plasma current I_p ramps up to 650 kA in about 400 ms. The safety factor profile (q) evolves during the initial current ramp-up and the central value (q_0) reaches unity shortly after the beginning of the current flat-top. Note that the equilibrium is reconstructed by EFIT code using data from magnetics and Thomson scattering system. Since the Motional Stark Effect (MSE) measurement was not available for this discharge, q profile and its temporal evolution are recomputed in TRANSP using a fixed boundary equilibrium code TEQ. As the estimated central q falls below unity, the sawtooth model in TRANSP (full reconnection model in this case) is applied at the measured sawtooth crash time. The signatures of sawtooth activity are clearly seen as repetitive spikes on data from magnetic fluctuation sensors located at the plasma edge on the low-field-side (figure 2(*e*)). Repetitive crashes also appear on the central electron density ($n_{e,0}$), temperature ($T_{e,0}$) and neutron rate measurements (figures 2(*c*) and (*f*)), which show measurable drops associated with each sawtooth event. $T_{e,0}$ and $n_{e,0}$ values stay around 1 keV and 2×10^{19} m^{-3} during sawtooth activities, respectively. Profiles are modulated around quasi-stationary values inside the sawtooth inversion radius, which is located around mid-radius at $R \approx 130$ cm (normalized minor radius ≈ 0.38). The drops in neutron rate indicate changes of thermal and/or fast ion profiles as about 90% of neutrons are generated by beam-target (thermal) reactions.
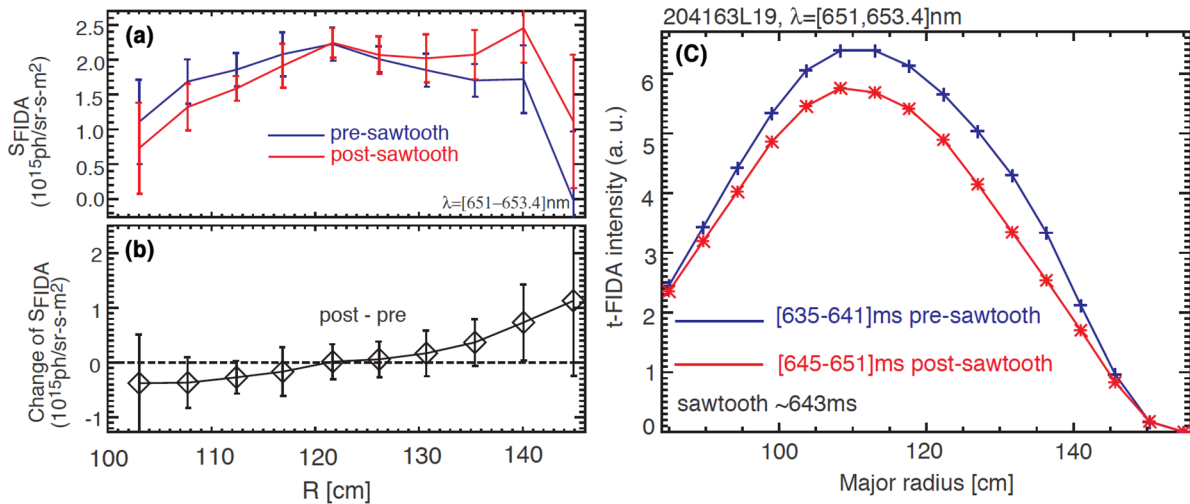
Figure 1. (*a*) Measured FIDA spatial profiles before (blue) and after (red) a sawtooth crash and (*b*) the relative change of signals. Note the FIDA data are conditional averaged over several sawtooth events. (*c*) Comparison of simulated FIDA spatial profiles calculated through the FIDAsim code using the plasma profiles and fast ion distribution from TRANSP with the partial reconnection model. Reproduced courtesy of IAEA. Figure from [9]. Copyright 2018 IAEA.
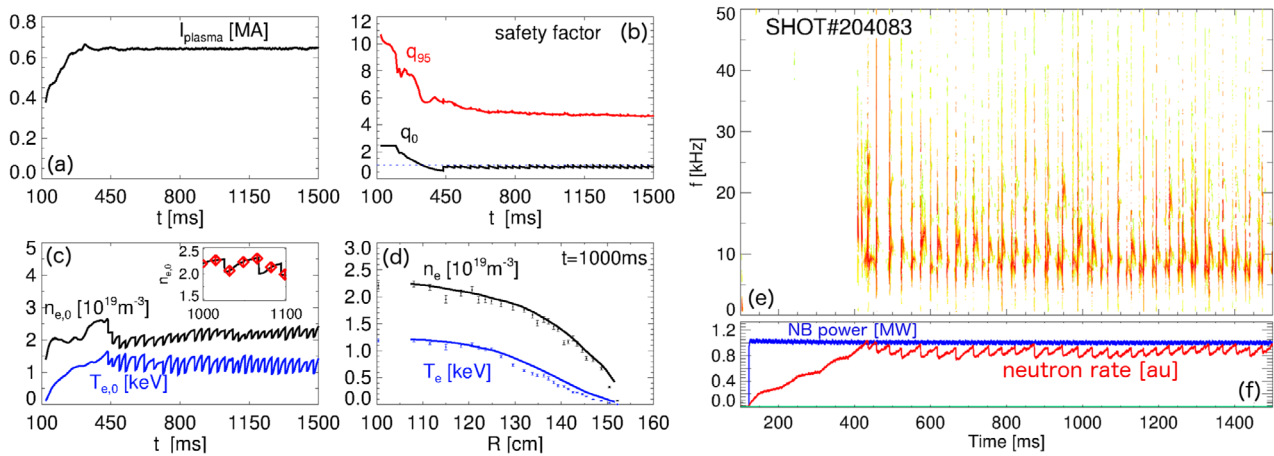

Figure 2. Experimental scenario for NSTX-U discharge #204083. (*a*) Plasma current in ramp-up and flat-top phase. (*b*) Evolution of central and edge values of the safety factor, as resulting from TRANSP simulation including sawtooth effects on the current profile. (*c*) Time evolution of reconstructed central electron density and temperature. The inset shows a subset of reconstructed electron density (solid line) and experimental points (red symbols). (*d*) Example of electron density and temperature profiles at $t = 1000$ ms. Symbols show the measured data and solid lines the profiles reconstructed through conditional average. (*e*) Spectrum of magnetic fluctuations from Mirnov coils at the plasma edge. Sawteeth are visible as spikes in the measured spectrum. (*f*) Time traces of injected NB power (blue) and measured neutron rate (red).

Since the sawtooth cycle duration is comparable to—or shorter than—the sampling time of the NSTX-U profile diagnostics, e.g. 16 ms for Thomson scattering system [17] and 10 ms for charge exchange recombination spectroscopy (CHERS) [18], available profile data are re-processed through conditional average to reconstruct the evolution of profiles on a finer time grid. Spikes in Mirnov coils' signals are first used to identify sawtooth events. Raw profile data from each sawtooth event are then re-binned on a 40 ms time basis synchronized with the time of crash. A fit of the average evolution at each radial location provides the characteristic recovery rate after the crash. Finally, the reconstructed recovery evolution is re-mapped for each crash over the entire discharge, using available (raw) data to rescale the amplitude of each crash.

Neutron counters' calibration on NSTX-U has typical uncertainties of $\pm10\%$ on the absolute values. To alleviate

the effect of uncertainties, calibration factors are adjusted to match the TRANSP predictions for MHD-free phases of the selected discharges, see for instance figure 2 before $t \sim 400$ ms. It should also be noted that *relative* changes in neutron rate (e.g. caused by sawteeth) are used throughout this work for the model/experiment comparison, thus reducing the effects of systematic uncertainties in the measured neutron rate.

3. Simulation methodology

3.1. Perturbation model

Simulations have been performed based on the NSTX-U discharge #204083 using the ORBIT code [14], a Hamiltonian guiding-center code for analyzing energetic particle transport by instabilities in tokamaks. The equilibrium from one time
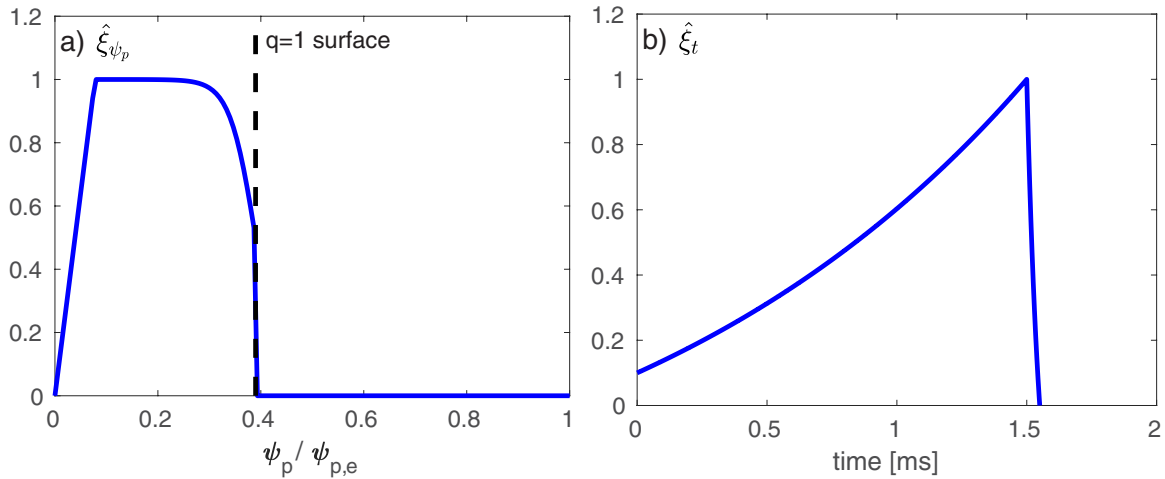
Figure 3. (*a*) Normalized radial displacement $\hat{\xi}_{\psi_p}$ profile. Black dashed line indicates unperturbed $q = 1$ surface. (*b*) Normalized temporal variation $\hat{\xi}_t$ on perturbation amplitude. Sawtooth crash is assumed to happen at 1.5 ms during 50 μs.

slice before a sawtooth crash (1093 ms) is extracted from an interpretative TRANSP run. The unperturbed initial distribution of Monte Carlo markers (position, pitch and energy) is also extracted from the NUBEAM module [19, 20] in TRANSP. The Monte Carlo module NUBEAM calculates the evolution of the energetic particle population based on neoclassical physics, including Coulomb collisions, slowing down on the thermal plasma and charge-exchange events [20]. In this work, the number of Monte Carlo particles is set to 10 000 to avoid time-consuming calculations while retaining enough statistics. Comparison with 20 000 particles shows less than 10% difference in the relative change of neutron rate (discussed in section 3.2) and in particular, for the larger mode amplitude, the difference is negligible. In order to take into account the sawtooth instability, a plasma displacement $\vec{\xi}$ has been used to represent the linearized perturbation on the magnetic field,

$$\delta B = \nabla \times \left(\vec{\xi} \times \vec{B} \right). \tag{1}$$

The radial component of $\vec{\xi}$ is defined as $\xi\left(\psi_{\mathrm{p}}, t, \theta, \zeta\right) = \Sigma \xi_{mn}\left(\psi_{\mathrm{p}}, t\right) \cos\left(n\zeta - m\theta - \omega t\right)$, where ξ_{mn} the radial perturbation profile, a product of the nominal amplitude $\xi_{0,mn}$, the normalized radial and temporal profiles $\hat{\xi}_{\psi_{\mathrm{p}},mn}$ and $\hat{\xi}_{t,mn}$, (m, n) and (θ, ζ) the poloidal and toroidal mode numbers and angles, respectively and ω the mode frequency. The radial and temporal profiles are taken from [21, 22] and are shown for a (1, 1) mode case in figure 3.

To avoid singularities in some of the field variables, cartesian coordinates (x, y) are used near the magnetic axis instead of (ψ, θ) in ORBIT. Since a (1, 1) mode perturbation can cause a displacement of the magnetic axis, the $\hat{\xi}_{\psi_{\mathrm{p}},mn}$ profile is modified to have zero perturbation on axis [23]. In addition, the perturbation outside the $q = 1$ surface (black dashed line) is set to zero. Note that the (1, 1) mode perturbation decreases quickly outside the $q = 1$ surface and the modification does not affect much on the simulation result (see figure 5(*a*)).

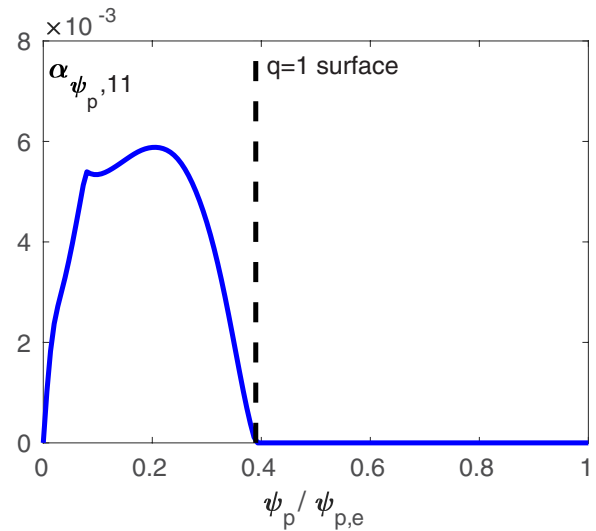In NSTX-U, the (1, 1) mode perturbation amplitude typically starts increasing about 1–2 ms before a sawtooth crash

Figure 4. The (1, 1) mode radial profile of α converted from $\hat{\xi}_{\psi_{\mathrm{p}}}$ using equation (3a). Perturbation is zero at the axis and outside the $q = 1$ surface (black dashed line).

and the crash duration is typically about $40 \sim 50$ μs. In this case, the amplitude is set to grow from 10% of the maximum amplitude and a sawtooth crash takes place at 1.5 ms during 50 μs. Full reconnection is assumed thus after the crash, the mode does not survive, i.e. the amplitude goes to zero. Note that during the evolution of the (1, 1) mode, the q profile is fixed.

In the ORBIT code, the magnetic perturbation is applied using a scalar function α instead of $\vec{\xi}$ and the perturbed magnetic field is obtained as

$$\delta \vec{B} = \nabla \times \left(\alpha \vec{B} \right). \tag{2}$$

Equation (2) brings the perturbed magnetic field equivalent to that from equation (1) in radial direction [24]. Since the radial component is the most important in this work and the other components are not used, it is acceptable to use the perturbation from α. Using the relation between α_{mn} and ξ_{mn} (equation
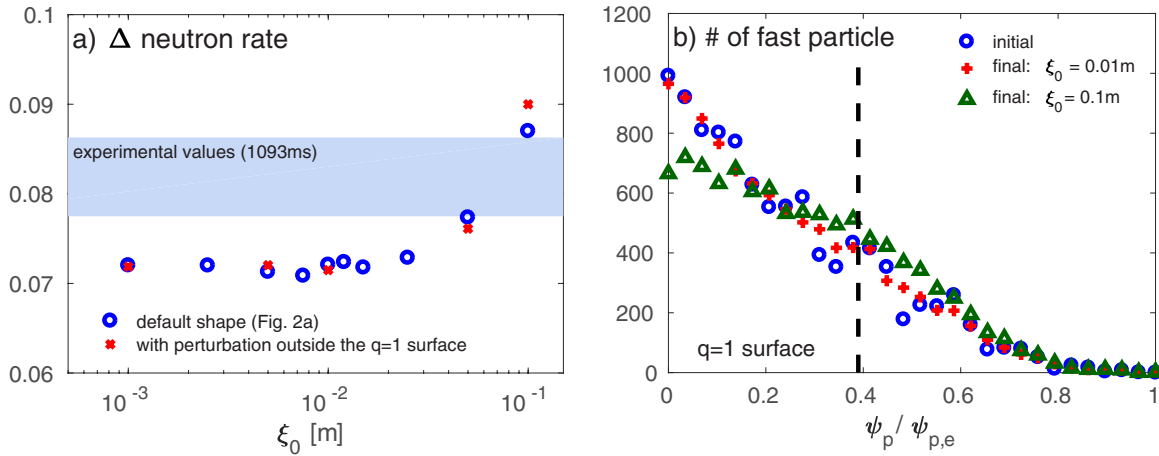
Figure 5. (*a*) The relative change of neutron rate is evaluated using equation (4) with different mode amplitudes (blue circle). When the mode amplitude is between 5.5 and 9.7 cm, simulation result is similar to that from experiment. The result is not sensitive to the perturbation shape. (*b*) With a smaller ξ_0 (red cross) fast particles keep the initial distribution (blue circle) while fast particles are redistributed by the perturbation with a larger amplitude (green triangle).

(3*a*)), the radial perturbed field is defined as equation (3*b*) [24].

$$\alpha_{mn} = \frac{m/q - n}{mg + nI}\xi_{mn}, \qquad (3a)$$

$$\delta\vec{B} \cdot \nabla\psi_{\mathrm{p}} = \sum_{m,n} \frac{mg + nI}{J}\alpha_{mn}\cos\left(n\zeta - m\theta - \omega t\right), \quad (3b)$$

where q the safety factor profile, g and I the poloidal and toroidal current functions, $\delta\vec{B}$ the perturbed magnetic field, ψ_{p} the poloidal magnetic flux and J the Jacobian. The α profile for the (1, 1) mode derived from $\hat{\xi}_{\psi_{\mathrm{p}}}$ in figure 3(*a*) with the perturbation amplitude ξ_0 of 7.5 cm is depicted in figure 4. The resultant profile has no perturbation at the axis and outside the $q = 1$ surface and the curve is similar to a simulation case in [22].

3.2. Determination of perturbation amplitude

The nominal amplitude $\xi_{0,mn}$ is a free parameter in the simulation. In order to find a proper range, the relative change of neutron rate with different $\xi_{0,mn}$ values, evaluated using the reaction rate for D–D reaction, $D + D \rightarrow {}^3\mathrm{He} + n$, is compared with the experimental measurement. The reaction rate is estimated using the deuterium density n_d, evaluated from the measured electron and carbon densities assuming quasineutrality and one impurity (carbon), and the volume element dV, the reaction cross section S and the square root of energy E of each particle from the ORBIT calculation at each fast particle position. Note that n_d is sum of the thermal deuterium $n_{d,t}$ and the deuterium beam $n_{d,f}$ densities since the beam particle density cannot be separately measured. From TRANSP simulations, $n_{d,f}$ is about 4% of $n_{d,t}$ (volume averaged value) so that n_d can be used for the measured $n_{d,t}$. The product of those parameters is summed over the number of test particle N and the reaction rate is evaluated before (subscript 0) and after (subscript f) a sawtooth crash, from which the relative change is obtained as seen in equation (4).

$$\Delta\mathrm{neut\_rate} = \frac{\sum_{k}^{N_0} n_{d0,k}S_{0,k}\sqrt{E_{0,k}}\mathrm{d}V_k - \sum_{k}^{N_f} n_{df,k}S_{f,k}\sqrt{E_{f,k}}\mathrm{d}V_k}{\sum_{k}^{N_0} n_{d0,k}S_{0,k}\sqrt{E_{0,k}}\mathrm{d}V_k}. \quad (4)$$

Using equation (4), the relative change of neutron rate induced by the (1, 1) mode perturbation is estimated for given amplitudes $\xi_{0,11}$ set between 0.1 and 10 cm and the simulation result (blue circle) is displayed in figure 5(*a*). The shaded region represents the relative change of neutron rate from the experimental measurement evaluated in the same way as equation (4), the difference between the neutron rate at the pre- and the post-crash divided by the pre-crash neutron rate. To reflect uncertainties in the calibration, the experimental value is given as a range. For small mode amplitude, fast particle orbits are only weakly affected and the neutron drop is entirely caused by redistribution of thermal ions, as seen in figure 5(*b*) (blue circle—without perturbation, red cross—application of 1 cm perturbation). As ξ_0 increases, fast particles are redistributed (see 10 cm perturbation, green triangle in figure 5(*b*)) and the relative change of neutron rate increases, reaching the experimental range for $5.5 \lesssim \xi_0 \lesssim 9.7$ cm. For the rest of the analysis, $\xi_0 = 7.5$ cm has been used.

As briefly mentioned above, the shape of perturbation near the $q = 1$ surface does not have a significant effect on the simulation result. The relative change of neutron rate for several amplitude cases are evaluated using the perturbation shape without cutting off the displacement outside the $q = 1$ surface. The result (figure 5(*a*) red cross) does not change within numerical uncertainties.

4. Simulation result

Using the perturbation shape and amplitude discussed in the previous section, the characteristics of sawtooth induced fast particle redistribution is investigated in this section. Although the amplitude is determined by comparison with experimental measurement, three different amplitudes ($\xi_0 = 0.1$, 1 and 10 cm) are initially used to verify if significant changes are
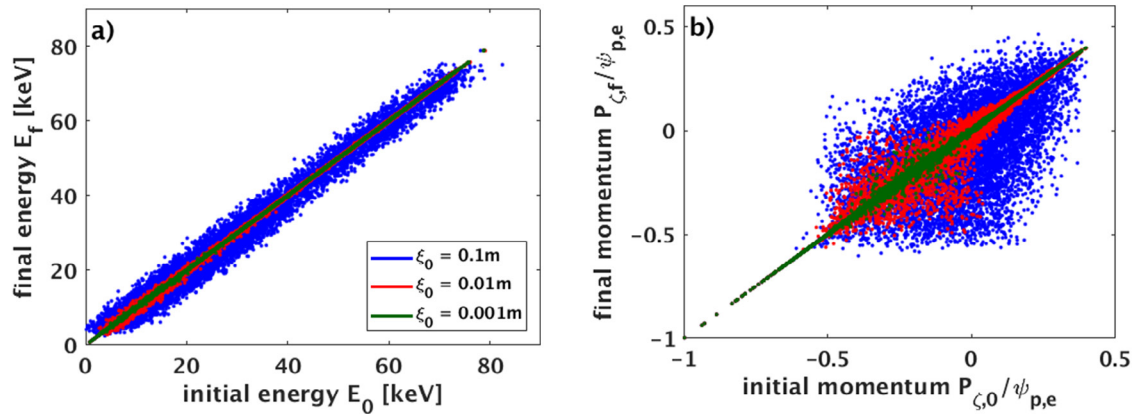
Figure 6. (*a*) Fast particle energy E and (*b*) normalized canonical angular momentum $P_{\zeta,N}$ variations are shown for three different perturbation mode amplitudes (blue, red and green for $\xi_0 = 10, 1, 0.1$ cm cases, respectively). Energy does not change while momentum shows significant variation with a larger amplitude.

observed in the fast particle energy and angular momentum induced by a sawtooth crash.

In figure 6, initial states of fast particle energy (E) and normalized canonical angular momentum ($P_{\zeta,N} = P_\zeta/\psi_{p,e}$, $\psi_{p,e}$ the poloidal magnetic flux at the edge) are shown versus the final states. With the smallest perturbation amplitude of 0.1 cm (green), E changes only about 1% while it shows larger variations of $10 \sim 60\%$ as the amplitude increases (red, blue), see figure 6(*a*). Compared to E, $P_{\zeta,N}$ in figure 6(*b*) features larger variations. With the smallest perturbation, the variation is about 2% but as the perturbation amplitude increases, the final $P_{\zeta,N}$ values vary more than 100% from the initial ones. This indicates that fast particles can be efficiently redistributed in phase space by a sawtooth crash with a sufficient amplitude. Note that the variation of $P_{\zeta,N}$ occurs mostly inside the sawtooth mixing radius around $P_{\zeta,N} = -0.5$ in this case, which depends on energy and pitch (ratio of parallel to total velocity). Although the variation is not significant, E is not conserved due to the finite electrostatic potential and mode frequency; low mode frequency results in the small variation of E relative to that of $P_{\zeta,N}$. Based on these results, further analysis focusing on the fast particle redistribution in phase space will be discussed for a fixed mode amplitude $\xi_0 = 7.5$ cm.

In order to find the characteristics of fast particle redistribution, orbit type classification of each particle is carried out first. The classification allows to identify the characteristic particle transport of each orbit type and the change of orbit type due to a sawtooth crash. Based on the initial energy and pitch, the orbit types of each particle are classified using the Hamiltonian equation of motion and the conservation of canonical angular momentum P_ζ [25]

$$E = \rho_\parallel^2 B^2/2 + \mu B + \Phi$$
$$P_\zeta = g\rho_\parallel - \psi_p \tag{5}$$

where $\rho_\parallel = v_\parallel/B$ the normalized parallel gyro radius, B the equilibrium magnetic field, $\mu = v_\perp^2/(2B)$ the magnetic moment, Φ the electrostatic potential. Using equation (5), the boundary of each particle type can be defined for a given particle energy (see figure 8). An example of classified orbit
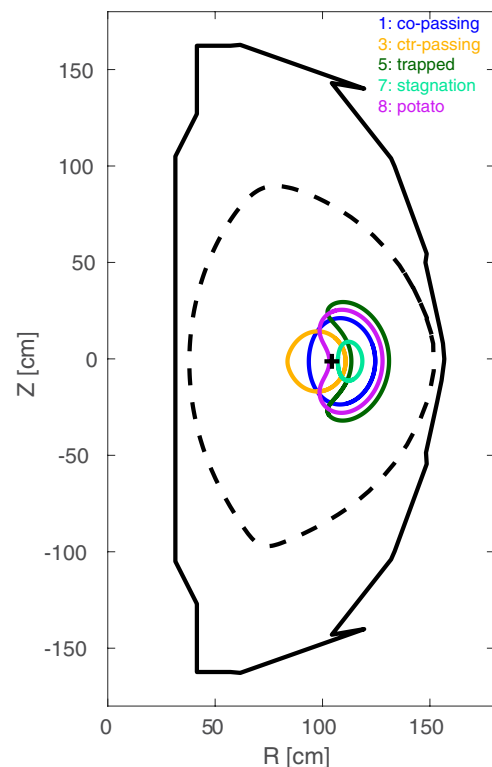

Figure 7. Trajectories of co-passing (blue), counter-passing (yellow), trapped (green), stagnation (light green) and potato (violet) types of particles with similar energy level of 40 keV. The black solid and dashed lines indicate NSTX-U limiter and plasma boundary, respectively and the black cross sign is the magnetic axis.

trajectories of particles with similar energy ($\sim$40 keV) is shown in figure 7. The trajectory of co-passing particle, moving around the magnetic axis (black cross) in the same direction to the plasma current, is displayed in blue and the particle moving in the opposite direction (counter-passing particle) is shown in yellow. Green, light green and violet lines indicate trapped, stagnation and potato particles, respectively. The last closed flux surface and NSTX-U limiter are shown in black dashed and solid lines, respectively. Note that these trajectories are obtained without perturbation and only confined particles are considered, i.e. lost particles are not displayed.
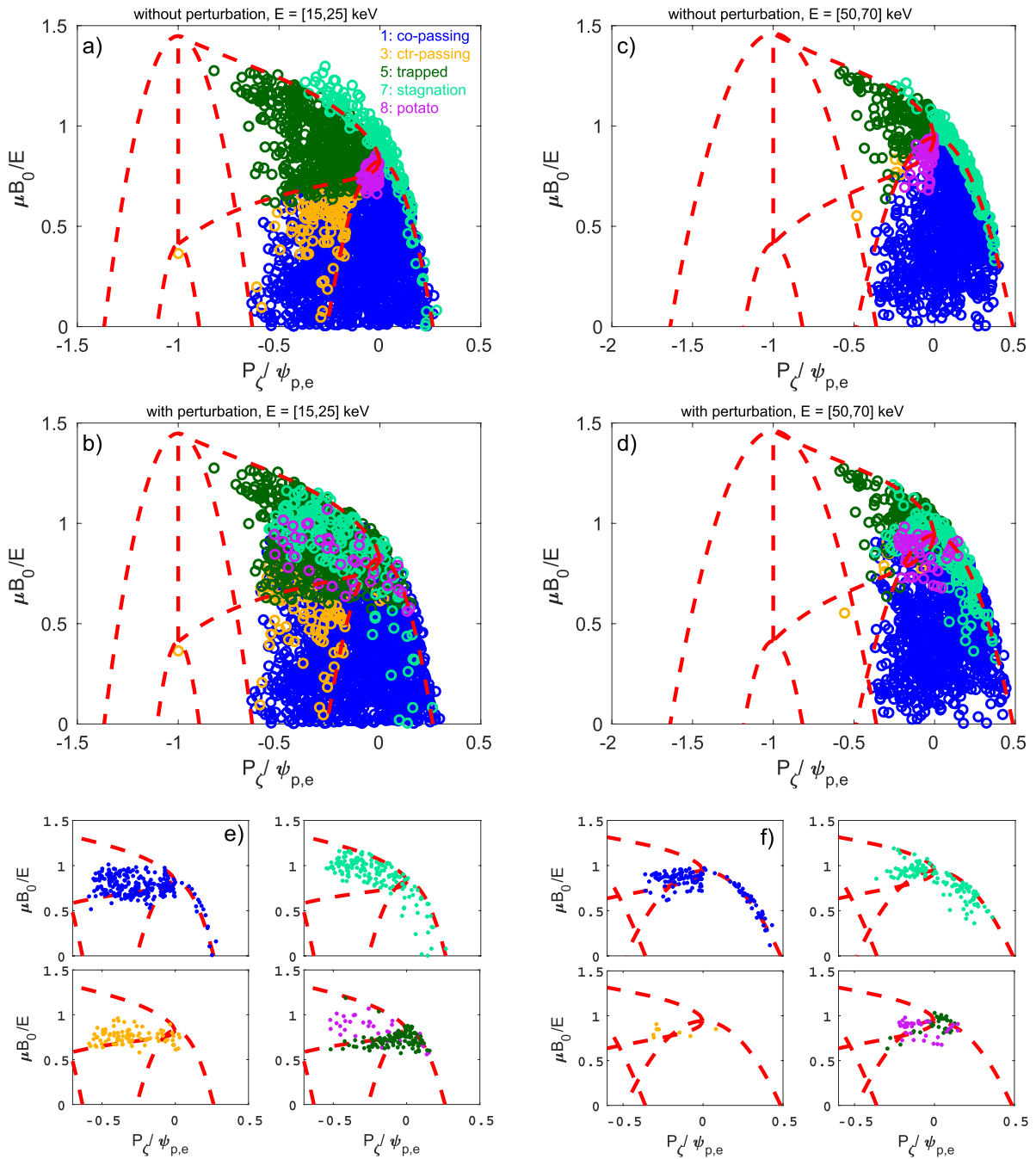
Figure 8. Fast particle distributions are shown for energy level of [15, 25] keV (*a*) without and (*b*) with the perturbation and for higher energy level [50, 70] keV (*c*) without and (*d*) with the perturbation. In (*e*) and (*f*), it is only shown particles with altered orbit types separated by their initial orbit type. For both without and with the perturbation cases, the initial orbit type is used to track the change of particle position and final orbit type. The orbit type boundaries, displayed as red dashed lines, are estimated using the average energy (20 and 60 keV). Initially without the perturbation, particles with each orbit type are well located in the boundaries but after the perturbation is applied, particles experience changes of position in phase space and the change of orbit type.

The orbit type numbers for confined particles are 1 for co-passing, 3 for counter-passing, 5 for trapped, 7 for stagnation and 8 for potato particles, while 2, 4 and 6 are for lost particles; co-passing, counter-passing and trapped, respectively.

4.1. Redistribution of fast particles in phase and real spaces

Using the classification of particle orbit types, the fast particle distribution in phase space is presented in figure 8. The

perturbation amplitude is set to $\xi_0 = 7.5$ cm and two different initial energy cases are shown. The left figures show the fast particle distribution without and with the perturbation (before and after a sawtooth crash) for the low energy case ([15, 25] keV), while the right ones refer to higher energy particles ([50, 70] keV). The horizontal axis is the normalized angular momentum $P_{\zeta,N}$ and the vertical one is the ratio of the magnetic moment to the particle energy. For the case with the perturbation, the initial orbit type is used for each particle thus
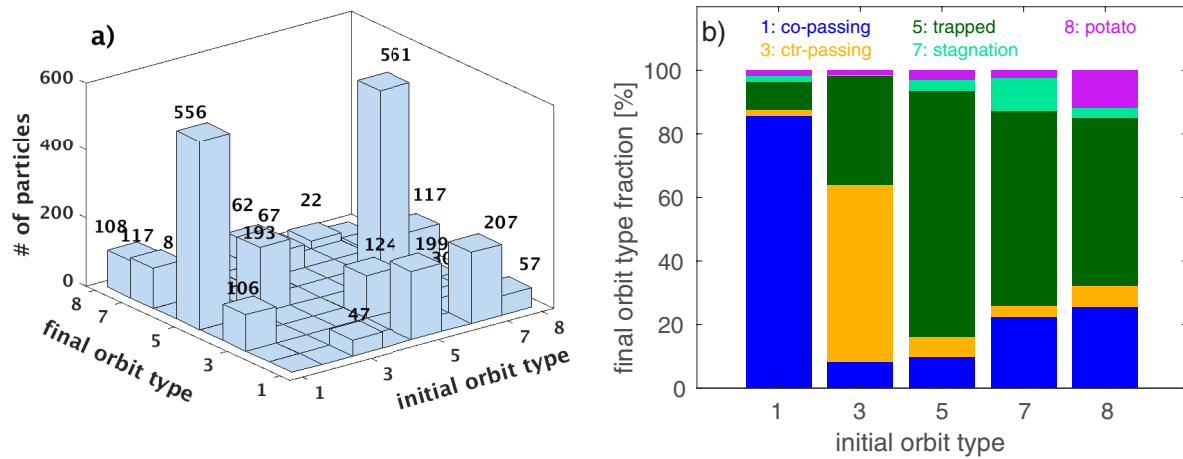
Figure 9. The change of orbit type after the sawtooth crash is quantitatively analysed as (*a*) set of initial and final orbit type (*i*,*f*) and (*b*) the fraction of each orbit type. (*i*,*f*) = (1,5) means initially co-passing particle turns into trapped particle after the crash. Most of case, particle orbits are converted to trapped particles while trapped particle becomes co- or counter-passing particles.

one can track the redistribution of particles. The classification boundaries are shown in red dashed lines in each figure for the average energy, i.e. 20 and 60 keV.

For both initial energy cases, without the perturbation particles with different orbit types are well localized within the orbit boundaries (the colors of particles for different orbit types are the same from figure 7). After a sawtooth crash, the orbit type is no longer consistent with the boundaries for some particles due to the redistribution. For example, stagnation particles (light green) are found outside trapped and co-passing particle boundaries but most of particles move inside trapped or co-passing particle boundaries, which means the particles' position in phase space and the orbit type are modified by the perturbation. In the bottom figures, particles whose orbit type is changed are shown for lower (figure 8(*e*)) and higher (figure 8(*f*)) energies. Each panel shows particles with different initial orbit type. For both energy cases, co-passing and stagnation particles are the most changed ones. These can be qualitatively compared with figure 9.

The investigation of redistribution of fast particle in phase space and the change of orbit topology are important as they allows to see how particles with different orbit types are differently affected by a sawtooth crash qualitatively and to better interpret/understand experimental data that show different behaviour for particles with different orbit types due to sawtooth [9].

Figure 8 shows the redistribution and orbit type change of fast particle in certain energy ranges. One can also find the change of orbit type quantitatively for all particles. Figure 9(*a*) shows the number of particles that change their orbit type during a sawtooth crash. Right and left axes are the initial and final orbit types and each block with number represents the number of particles with the given initial and final orbit type set. For instance, an initial and final orbit type set (1,5) and the corresponding number 556 mean that 556 initially co-passing particles turn into trapped particles after the crash. Among the 10 000 particles about 26% particles experience orbit type change and the largest changes are found from co-passing and stagnation to trapped particles. In addition, a large

portion of counter-passing and potato particles also turn into trapped particles while trapped particles mostly become co- or counter-passing particles. Note that in this figure the particles that keep their initial orbit types are not shown.

In figure 9(*b*), the fraction of each orbit type after the crash is displayed versus the initial orbit type. As seen in figure 8, most of co-passing (∼85%) and trapped (∼77%) particles keep their initial orbit type while other types of particles have significant fractions of changed orbit type, mostly turning into trapped particles (∼35% of counter-passing, ∼60% of stagnation, ∼53% of potato particles). Stagnation and potato particles are located in just outside or between boundaries of different orbit types, thus it is easier to change their orbit type and the fraction of modified orbit type is much larger compared to passing and trapped particles. Note that only about 9% of co-passing particles become trapped particle after the crash. However the total number of co-passing particles is the largest and the 9% makes the similar number of change as stagnation case as shown in figure 9(*a*).

Similar to the effect of sawtooth crash on fast ion redistribution in phase space, the modification of fast ion distribution can also be seen in real space depending on the orbit type. The number of passing and trapped particles evaluated at each counting bin across the flux surfaces are shown in figure 10. To improve the statistics, the number of particle is accumulated over 10 μs with zero perturbation amplitude to complete a few orbits before and after a sawtooth crash. Figures 10(*a*) and (*b*) show the initial (blue circle) and final (red cross) number of particles at each counting bin for co- and counter-passing particles while those of trapped and stagnation particles are depicted in figures 10(*c*) and (*d*). Note that particles are classified based on their initial orbit type for both initial and final profiles, so that those figures show the redistribution of the initial types of particles in real space regardless the final orbit type.

Co- and counter-passing particles are centrally peaked before a crash and due to the perturbation, centrally located particles move outside the *q* = 1 surface (black dashed line) after the crash. The final status of co- and counter-passing
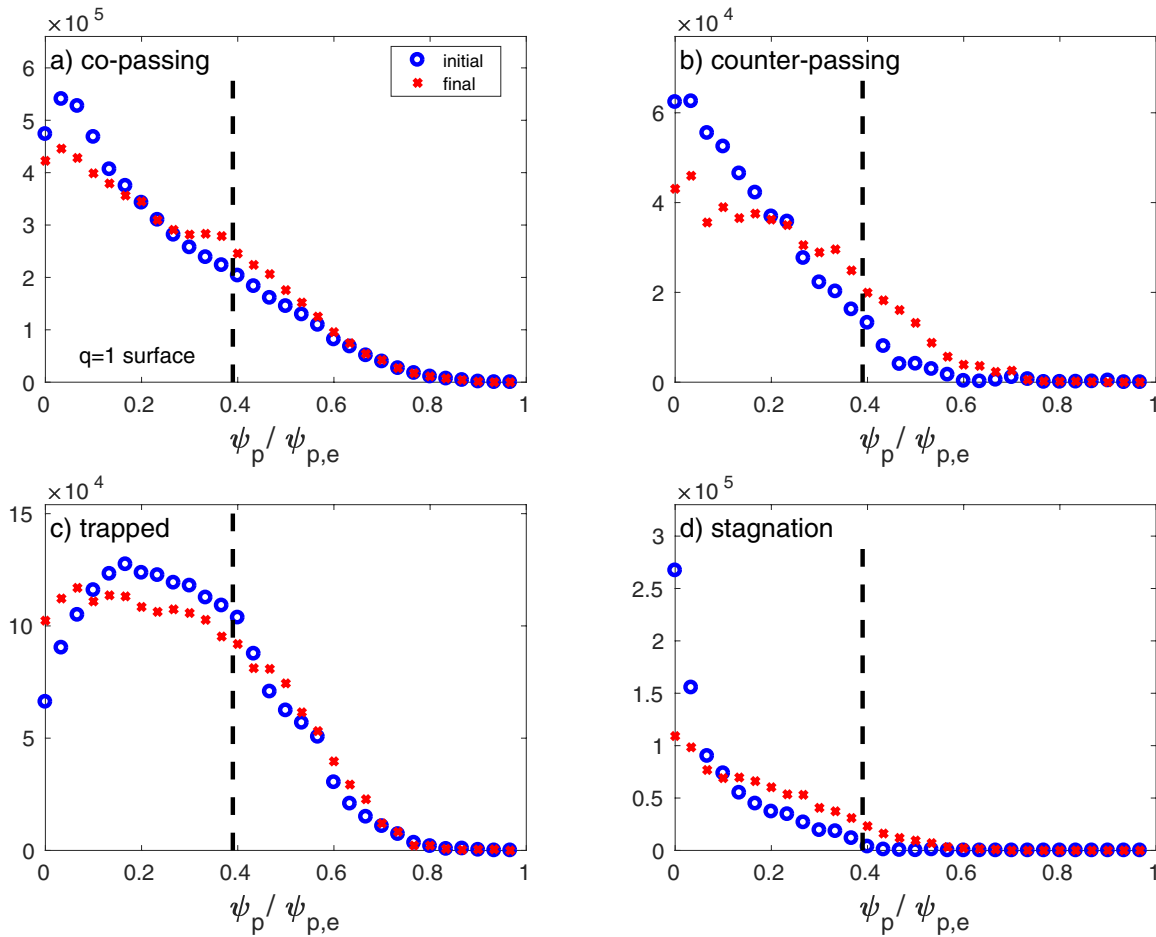
Figure 10. Number of particle at each counting bin before (blue circle) and after (red cross) a sawtooth crash for (*a*) co-passing, (*b*) counter-passing, (*c*) trapped and (*d*) stagnation particles. Passing particles show the clear redistribution induced by sawtooth while the final state of trapped particles does not give a clear sign of sawtooth effect. Stagnation particles are expected to have similar redistributions to trapped particles but their behaviour is close to passing particles. It is different from [26] and needs more investigation. The sawtooth inversion radius for passing particles is located near $\psi_p/\psi_{p,e} \sim 0.25$ while $\psi_p/\psi_{p,e} \sim 0.1$ for trapped and stagnation particles.

particle show the clear effect of the sawtooth instability. However, trapped particles show a different behaviour compared to passing particles. Initially trapped particles have a broader profile and a hollow region in the center. After the crash, the profile is modified but sawtooth induced redistribution outside the $q = 1$ surface is not clearly seen as for passing particles. Stagnation and trapped particles have similar characteristics such as pitch thus it is expected that the redistribution of stagnation particles may be comparable to that of trapped ones as shown in [26]. However, stagnation particles in the center are expelled and are accumulated outside $\psi_p/\psi_{p,e} \sim 0.1$, alike passing particles rather than trapped particles (figure 10(*d*)). Since the sawtooth induced redistribution is described using $\vec{E} \times \vec{B}$ in [26] while radial displacement is directly applied in this work, stagnation particles may undergo a different dynamic. For instance, compared to the case in [26], trapped and stagnation particles have a much larger range of pitch. In order to compare the models and to understand better the characteristics of fast particles, more investigation would be needed.

The simulation results show that passing particles are more significantly affected by sawtooth instability than trapped particles. One likely explanation is the dependence of the

redistribution process on fast ion energy. Based on the criteria for sawtooth induced redistribution [13], the critical initial energies of passing and trapped particles for redistribution are evaluated for this discharge. The critical energy for passing particles varies depending on the particles' pitch and can be $60 \sim 70$ keV to a few hundred keV while about 30 keV for trapped particles. The minimum and maximum particle energies are about 10 and 100 keV. Therefore, the majority of passing particles have energies below the critical energy and may be redistributed by the sawtooth, whereas only trapped particles that have energy similar or lower than 30 keV are mostly affected. Note that as the criteria are for passing and trapped particles, the critical energy for stagnation particles is not discussed here.

These results are qualitatively consistent with the experimental observation from similar NSTX-U discharges, see [9]. As already mentioned, the effects of sawtooth on different orbit types are not taken into consideration in the current sawtooth model in TRANSP when the model is applied to the fast ion redistribution. Therefore, even if TRANSP simulations can reproduce experimental neutron rates using an ad hoc set of free parameter, the details of the fast ion distribution evolution can be different. For instance, the experimental measurement
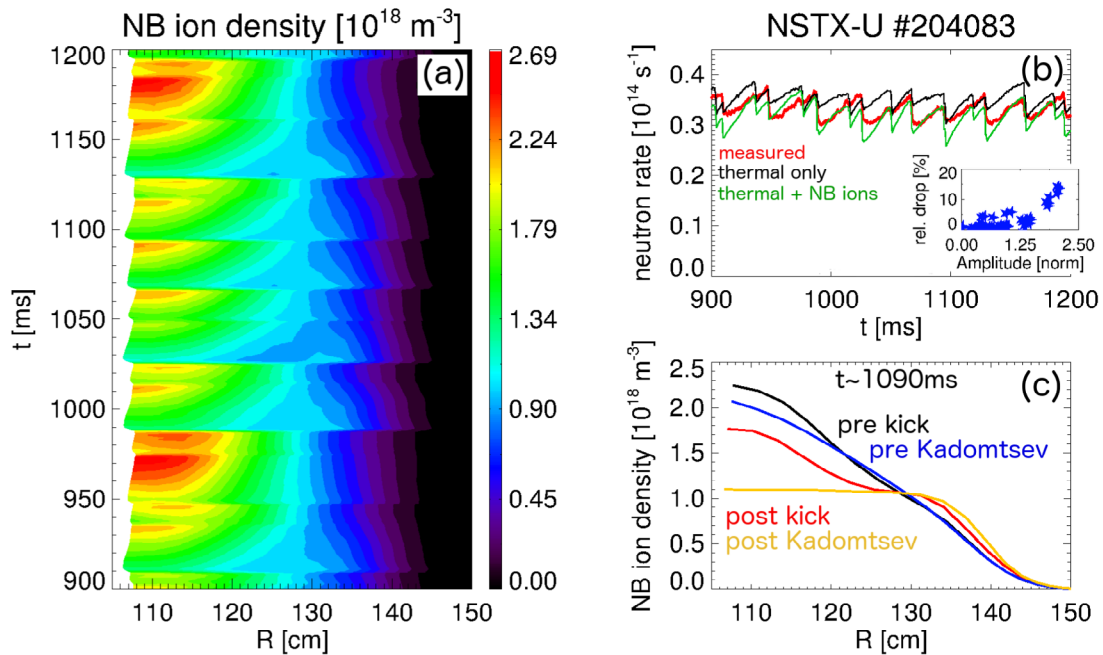
Figure 11. (*a*) NB ion density evolution versus time and radius. (*b*) Measured neutron rate (red) compared with TRANSP results that include variations of thermal profiles only (black) and of thermal plus NB ion profiles (Green). The inset shows the contribution to the relative drop in neutron rate caused by NB ion transport as the amplitude of the sawtooth events is increased in the simulation. (*c*) NB ion density profiles from TRANSP just before and after a sawtooth crash using the kick model (black, red) and the full reconnection model (blue, yellow) implemented in TRANSP. Note the formation of a 'shoulder' across the inversion radius, $R \approx 130$ cm, which reminds the experimental observations from FIDA for co-passing fast ions [9].

of fast ion profiles from tangential FIDA system mostly sensitive to co-passing fast ions shows a clear effect of sawtooth, while the FIDA simulation result based on TRANSP simulations that reproduce the experimental neutron rate is not consistent with the measurement and the effect of sawtooth around the inversion radius is not clear [9].

4.2. Preliminary test for the application of ORBIT modeling to TRANSP

The ORBIT results discussed previously indicate that fast ion transport by sawteeth has complicated dependencies on the fast ion phase space variables, which cannot be represented through a simple, zero-dimensional analysis. Referring to future burning plasmas, the fast particle distribution function is expected to be a complicated function of phase space, with fast ions from alpha reactions, NB injection and—possibly—RF waves in the ion cyclotron range of frequency. Therefore, it seems likely that a comprehensive fast ion transport model must have phase space resolution to correctly recover the effects of sawteeth.

To test this idea, the reduced *kick model* [15, 16] for fast ion transport presently implemented in TRANSP is used in conjunction with results from the ORBIT modeling. The kick model is based on 'transport probability matrices' to represent the fast ion transport by instabilities in the Monte-Carlo NUBEAM module of TRANSP. The matrices are computed from either numerical simulations (e.g. through ORBIT) or theory. In essence, each matrix represents the probability that fast ions from a certain (E, P_ζ, μ) region in phase space will experience changes—or *kicks*—in energy and P_ζ by an instability during

their orbiting over a certain time interval. For this work, the same ORBIT framework discussed above is used to compute a probability matrix associated with the sawtooth.

As discussed in section 2, the experimental data available for the sawtoothing L-mode scenario during the NSTX-U commissioning phase present large uncertainties. Therefore, these initial TRANSP simulations should be intended as an exploratory work rather than as a detailed, quantitative analysis of the actual experiment. For example, simulations shown in figure 11(*b*) indicate that most of the drop in the measured neutron rate may actually be caused by sawtooth-induced changes in the thermal plasma profiles. Simulations that include the reconstructed profiles, but do not evolve the fast ion population, achieve neutron rate drops that are (on average) comparable to the measured ones.

Nevertheless, the simulation results also show a potential improvement of the sawtooth models presently implemented in TRANSP. Figure 11(*a*) shows the evolution of the NB ion density profile from TRANSP simulations using the kick model to mimic sawtooth effects on NB ions. One main conclusion is that the kick model can account for more variability in the NB ion density profile after a crash compared to the standard sawtooth model in TRANSP (Kadomtsev model in this case) as seen in figure 11(*c*). Profiles modified according to the Kadomtsev model are assumed to flatten inside the inversion radius (see yellow curve in figure 11(*c*)) at each crash. The kick model allows more flexibility, e.g. in mimicking partial reconnection which may result in the incomplete redistribution of fast particles. In addition, while both the Kadomtsev and kick models cause a drop of central profile and an increase outside the inversion radius, the effects on the fast ion distribution can in
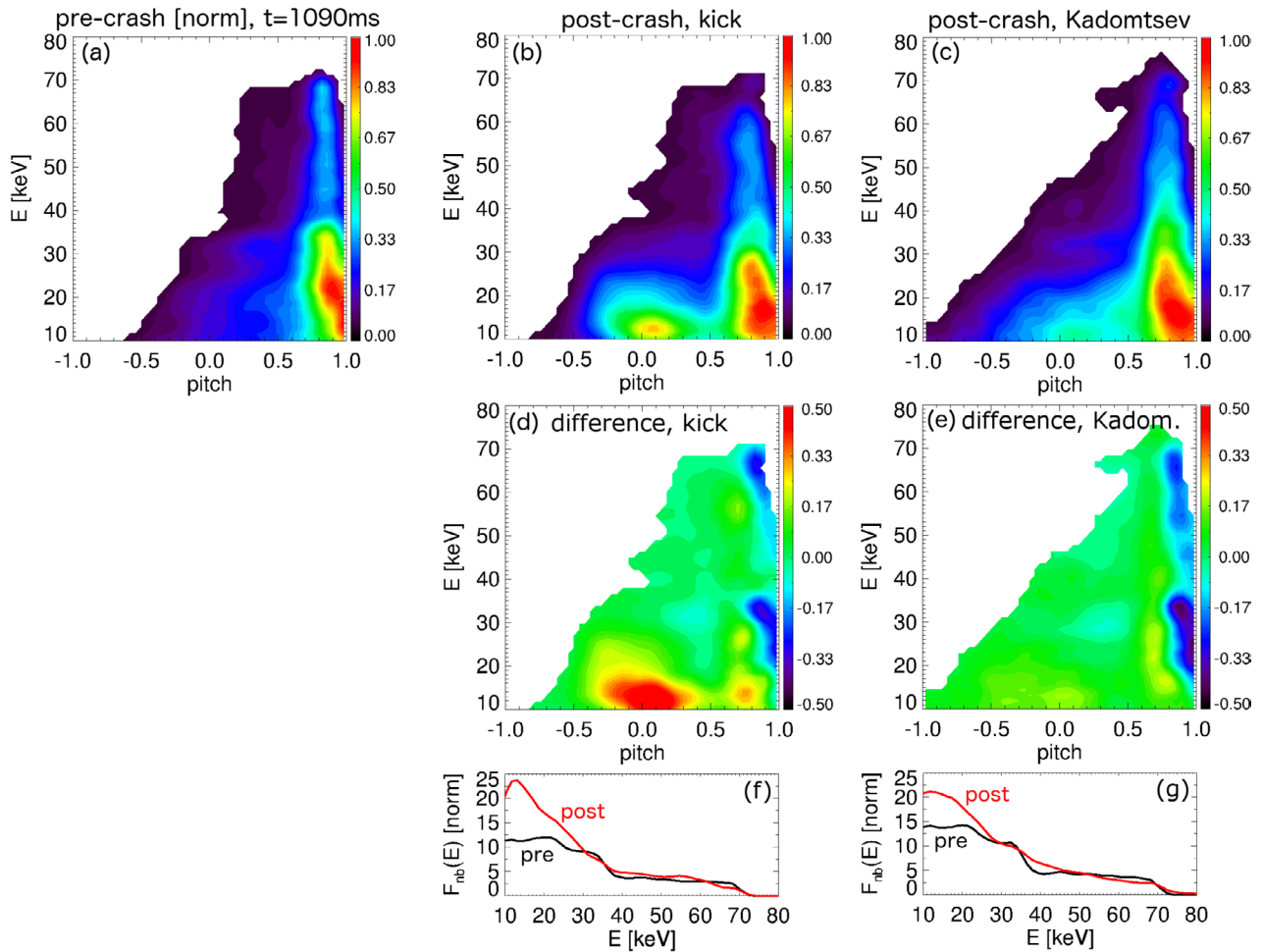
Figure 12. NB ion distributions from TRANSP as a function of energy and pitch. Distributions are sampled around $R \approx 135$ cm, corresponding to $\Psi_p/\Psi_{p,e} = 0.5$. (*a*) Distribution before a sawtooth crash, $t \sim 1090$ ms. ((*b*) and (*c*)) Distribution after the crash as computed using the kick model or the standard Kadomtsev model, respectively. The colour scale in (*a*) is normalized to the maximum value and the same normalization is used for (*b*) and (*c*). ((*d*) and (*e*)) Difference in distribution after and before the crash. (*f*) and (*g*) Distributions integrated over pitch for the two cases.

principle be quite different and explain the mismatch between FIDA measurements and simulations reported in [9]. Note that although the sawtooth crash timing is the same for the two simulations, the evolution between crashes can be different depending on the post-crash profiles. Therefore, the pre-crash profiles using kick and Kadomtsev models in figure 11(*c*) are not identical.

Figure 12 shows the NB ion distribution just outside the $q = 1$ location ($R \approx 135$ cm) before and after a crash (see figure 11(*c*)). Differences between the two models are observed in the general shape of the post-crash distribution, although the density profiles at this location are comparable. In particular, the kick model predicts an *increase* in the distribution for pitch $\gtrsim 0.5$ and energies $\gtrsim 30$ keV, i.e. the range sampled by the tangential FIDA system, whereas the Kadomtsev model computes an overall decrease. This general features appear (at least) consistent with experimental observations from FIDA [9] and suggest that the kick model can recover features not included in the present models. A closer comparison with the measurements is beyond the scope of this work, since it would require improved profile diagnostics with

a higher sampling rate to reduce the experimental uncertainties in the reconstructed profiles.

5. Conclusion

Modeling of sawtooth discharge helps to understand/interpret experimental results and to set an operation scenario with a prediction of behaviour of sawtooth instability. In order for the sawtooth modeling to provide more reliable prediction, the characteristics of fast ion transport should be taken into consideration. As the first step of the development of a comprehensive model for fast ion transport induced by a sawtooth crash, modeling using the ORBIT code is performed based on a NSTX-U sawtoothing discharge to find the effect of sawtooth instability and the phase space dependence on fast ion redistribution.

The sawtooth instability can be applied to the ORBIT code by implementing linear plasma displacement as the displacement induces perturbed magnetic fields. The normalized radial profile of the given displacement is modified to have zero amplitude at the magnetic axis to avoid an intrinsic

numerical problem of the ORBIT code. The normalized temporal profile is defined with characteristic times of NSTX-U sawtoothing discharges. The nominal amplitude of the displacement is determined by the comparison with experimental measurement of neutron rate. Since the ORBIT code does not provide direct calculation of neutron rate, the relative change of neutron rate before and after a sawtooth crash is used for the comparison.

The effect of sawtooth crash is investigated in phase space for different fast ion orbit types. Due to the application of perturbation, both energy and canonical angular momentum of fast ion are not conserved although the change of particle energy before and after a sawtooth crash is not significant. With a sufficiently large perturbation amplitude, particles are redistributed by sawtooth in phase space. Orbit types are also modified. Most of co-passing and trapped particles keep their orbit type while large fractions of counter-passing, stagnation and potato particles turn into trapped particles due to the perturbation.

The redistribution of fast ions in real space indicates that passing particles are more affected by sawtooth than trapped particles. The number of co- and counter-passing particles at each counting bin show the clear effect of sawtooth crash, the centrally located particles move out after the crash. Trapped particles distribution is also modified by a sawtooth crash but the result is not as clear as the passing particle case. The different behaviour of passing and trapped particles are qualitatively consistent with the experimental measurements. This might be because of the different critical energies from the criteria for sawtooth induced redistribution [13]. For the conditions investigated in this work, passing particles have a critical energy 60 keV or larger depending on particles' pitch, thus most particles are affected by sawtooth. Fewer trapped particles are influenced as their critical energy is about 30 keV. The criteria introduced in a theoretical work can be useful to compare with simulation results and to find characteristics of fast ion transport during a sawtooth crash. Therefore, more effective way to compare with the theory need to be applied as well as an improved sawtooth modeling that includes more physics and is more reliable is required beyond simple zero-dimensional prediction.

The initial TRANSP simulation result that applies the kick model combined with the ORBIT modeling shows a potential improvement of the present sawtooth model. Although the neutron rate is in disagreement with the measurement, the NB ion density after a crash is consistent with the FIDA data. Clearly, more work is required to explore the potential of the kick model (or a derived version of it) for improvements over the existing sawtooth models in TRANSP. To overcome the limitations of diagnostic data from the NSTX-U commissioning campaign, diagnostic improvements are under way for kinetic profile diagnostics in view of the next NSTX-U campaign. Upgrades to the CHERS system will result in a four-fold reduction in sampling rate, thus allowing a 2.5 ms time resolution for full radial profiles of ion density, temperature and toroidal rotation. A new pulsed Thomson scattering system is being installed to achieve a time resolution $\leqslant 1$ ms for electron density and temperature. In the short term, data from other devices would also prove useful for further model validation and development.

Acknowledgments

ORCID iDs

D. Kim ⓘ https://orcid.org/0000-0002-6085-9525
M. Podestà ⓘ https://orcid.org/0000-0003-4975-0585
D. Liu ⓘ https://orcid.org/0000-0001-9174-7078
F.M. Poli ⓘ https://orcid.org/0000-0003-3959-4371

References

[1] Porcelli F., Boucher D. and Rosenbluth M.N. 1996 *Plasma Phys. Control. Fusion* **38** 2163
[2] Sauter O. *et al* 2002 *Phys. Rev. Lett.* **88** 105001
[3] Menard J. *et al* 2012 *Nucl. Fusion* **52** 083015
[4] Ono M. *et al* 2000 *Nucl. Fusion* **40** 557
[5] Menard J. *et al* 2017 *Nucl. Fusion* **57** 102006
[6] Battaglia D. *et al* 2018 *Nucl. Fusion* **58** 046010
[7] Hawryluk R. 1980 *An Empirical Approach to Tokamak Transport Physics Close to Thermonuclear Conditions* vol 1, ed B. Coppi *et al* (Brussels: Commission of the European Communities) p 19 (http://w3.pppl.gov/~pshare/help/transp.htm)
[8] Kadomtsev B. 1975 *Sov. J. Plasma Phys.* **1** 710
[9] Liu D. *et al* 2018 Effect of sawtooth crashes on fast ion distribution in NSTX-U *Nucl. Fusion* **58** 082028
[10] Bortolon A., Heidbrink W. and Podestà M. 2010 *Rev. Sci. Instrum.* **81** 10D728
[11] Podestà M., Heidbrink W., Bell R. and Feder R. 2008 *Rev. Sci. Instrum.* **79** 10E521
[12] Heidbrink W.W., Liu D., Luo Y., Ruskov E. and Geiger B. 2011 *Commun. Comput. Phys.* **10** 716
[13] Kolesnichenko Y.I., Lutsenko V. and Yakovenko Y.V. 1997 *Phys. Plasmas* **4** 2544
[14] White R. and Chance M.S. 1984 *Phys. Fluids* **27** 2455
[15] Podestà M., Gorelenkova M. and White R. 2014 *Plasma Phys. Control. Fusion* **56** 055003
[16] Podestà M., Gorelenkova M., Gorelenkov N. and White R. 2017 *Plasma Phys. Control. Fusion* **59** 095008
[17] LeBlanc B. 2008 *Rev. Sci. Instrum.* **79** 10E737
[18] Bell R. *et al* 2010 *Phys. Plasmas* **17** 082507
[19] Goldston R. *et al* 1981 *J. Comput. Phys.* **43** 61
[20] Pankin A. *et al* 2004 *Comput. Phys. Commun.* **159** 157
[21] Farengo R. *et al* 2013 *Nucl. Fusion* **53** 043012
[22] Zhao Y. and White R. 1997 *Phys. Plasmas* **4** 1103
[23] White R. 2017 private communication
[24] White R. 2013 *Phys. Plasmas* **20** 022105
[25] White R. 2014 *The Theory of Toroidally Confined Plasmas* 3rd edn (London: Imperial College Press)
[26] Weiland M. *et al* 2016 *Plasma Phys. Control. Fusion* **58** 025012